



**HAL**  
open science

## Resonant Oscillations of Josephson Current in Nb-Bi 2 Te 2.3 Se 0.7 -Nb Junctions

Vasily S Stolyarov, Dimitri Roditchev, Vladimir L Gurtovoi, Sergey N Kozlov,  
Dmitriy S Yakovlev, Olga V Skryabina, Valerii M Vinokur, Alexander A  
Golubov

► **To cite this version:**

Vasily S Stolyarov, Dimitri Roditchev, Vladimir L Gurtovoi, Sergey N Kozlov, Dmitriy S Yakovlev, et al.. Resonant Oscillations of Josephson Current in Nb-Bi 2 Te 2.3 Se 0.7 -Nb Junctions. *Advanced Quantum Technologies*, 2022, pp.2100124. 10.1002/qute.202100124 . hal-03557430

**HAL Id: hal-03557430**

<https://hal.sorbonne-universite.fr/hal-03557430v1>

Submitted on 4 Feb 2022

**HAL** is a multi-disciplinary open access archive for the deposit and dissemination of scientific research documents, whether they are published or not. The documents may come from teaching and research institutions in France or abroad, or from public or private research centers.

L'archive ouverte pluridisciplinaire **HAL**, est destinée au dépôt et à la diffusion de documents scientifiques de niveau recherche, publiés ou non, émanant des établissements d'enseignement et de recherche français ou étrangers, des laboratoires publics ou privés.

# Resonant Oscillations of Josephson Current in Nb-Bi<sub>2</sub>Te<sub>2.3</sub>Se<sub>0.7</sub>-Nb Junctions

Vasily S. Stolyarov,\* Dimitri Roditchev, Vladimir L. Gurtovoi, Sergey N. Kozlov, Dmitriy S. Yakovlev, Olga V. Skryabina, Valerii M. Vinokur, and Alexander A. Golubov

Josephson proximity junctions and devices employing topological insulators are promising candidates for realizing topological superconductivity and topologically protected quantum circuits. Here, the new type of oscillations of the critical Josephson current in the ballistic Nb-Bi<sub>2</sub>Te<sub>2.3</sub>Se<sub>0.7</sub>-Nb junctions subject to the magnetic fields is reported. The oscillations appear below  $\approx 400$  mK and have a very unusual sharp-peaked shape. Their ultra-short period  $\approx 1$  Oe, by orders of magnitude shorter than the expected periodicity due to fluxoid quantization in the device, corresponds to the extremely low energy scale  $\approx 1$   $\mu$ eV. It is established that the observed effect is due to the resonant transmission of Andreev quasiparticles via the peculiar energy levels forming near the S-TI interfaces.

experimental groups have already realized the S-TI interfaces and S-TI-S junctions, and studied the Josephson current across them, see refs. [13–20] and references therein. A few papers has reported unusual Shapiro steps consistent with the formation of the *p*-wave correlations.<sup>[21,22]</sup> Here we report on the ultra-fast oscillations of the Josephson current in the magnetic field revealed in the mesoscopic S-TI-S devices comprising single nano-crystals of Bi<sub>2</sub>Te<sub>2.3</sub>Se<sub>0.7</sub>. We propose that these oscillations result due to formation of the peculiar Andreev bound states with the very peculiar fine structure of the energy levels at the S-TI contacts. This picture concurs with the possibility of the induced *p*-wave

superconducting order due to the combination of the conventional *s*-wave superconducting correlations with the peculiar symmetry of the used TI.

## 1. Introduction

The concept of *p*-wave superconductivity<sup>[1]</sup> harboring a trove of exotic topological states<sup>[2–5]</sup> was put forth nearly 60 years ago. Recent proposals<sup>[6,7]</sup> of inducing it by sandwiching a trivial *s*-wave superconductor (S) with a topological insulator (TI) triggered a burst of a research activity. Various models focused on the possible pairing symmetries of the superconducting order induced by proximity to topological layers.<sup>[8–12]</sup> Several

## 2. Results

The DC-transport measurements (see Experimental Section and Supporting Information section “Details of the Transport Mea-

V. S. Stolyarov, D. Roditchev, V. L. Gurtovoi, S. N. Kozlov, D. S. Yakovlev, O. V. Skryabina, A. A. Golubov  
Center for Advanced Mesoscience and Nanotechnology  
Moscow Institute of Physics and Technology  
Dolgoprudny, Moscow 141700, Russia  
E-mail: vasily.stolyarov@gmail.com

V. S. Stolyarov  
Dukhov Research Institute of Automatics (VNIIA)  
Moscow 127055, Russia

V. S. Stolyarov  
National University of Science and Technology MISIS  
Moscow 119049, Russia

D. Roditchev, S. N. Kozlov  
Laboratoire de Physique et d'Étude des Matériaux (LPEM), UMR-8213  
ESPCI Paris  
PSL Research University  
CNRS  
Sorbonne Université  
Paris 75005, France

V. L. Gurtovoi  
Institute of Microelectronics Technology RAS  
Chernogolovka 142432, Russia

O. V. Skryabina  
Institute of Solid State Physics RAS  
Chernogolovka 142432, Russia

V. M. Vinokur  
Terra Quantum AG  
St. Gallerstrasse 16A, Rorschach CH-9400, Switzerland

V. M. Vinokur, A. A. Golubov  
Faculty of Science and Technology and MESA+ Institute of  
Nanotechnology  
University of Twente  
Enschede, AE 7500, The Netherlands

 The ORCID identification number(s) for the author(s) of this article can be found under <https://doi.org/10.1002/qute.202100124>

© 2022 The Authors. Advanced Quantum Technologies published by Wiley-VCH GmbH. This is an open access article under the terms of the Creative Commons Attribution-NonCommercial-NoDerivs License, which permits use and distribution in any medium, provided the original work is properly cited, the use is non-commercial and no modifications or adaptations are made.

DOI: 10.1002/qute.202100124

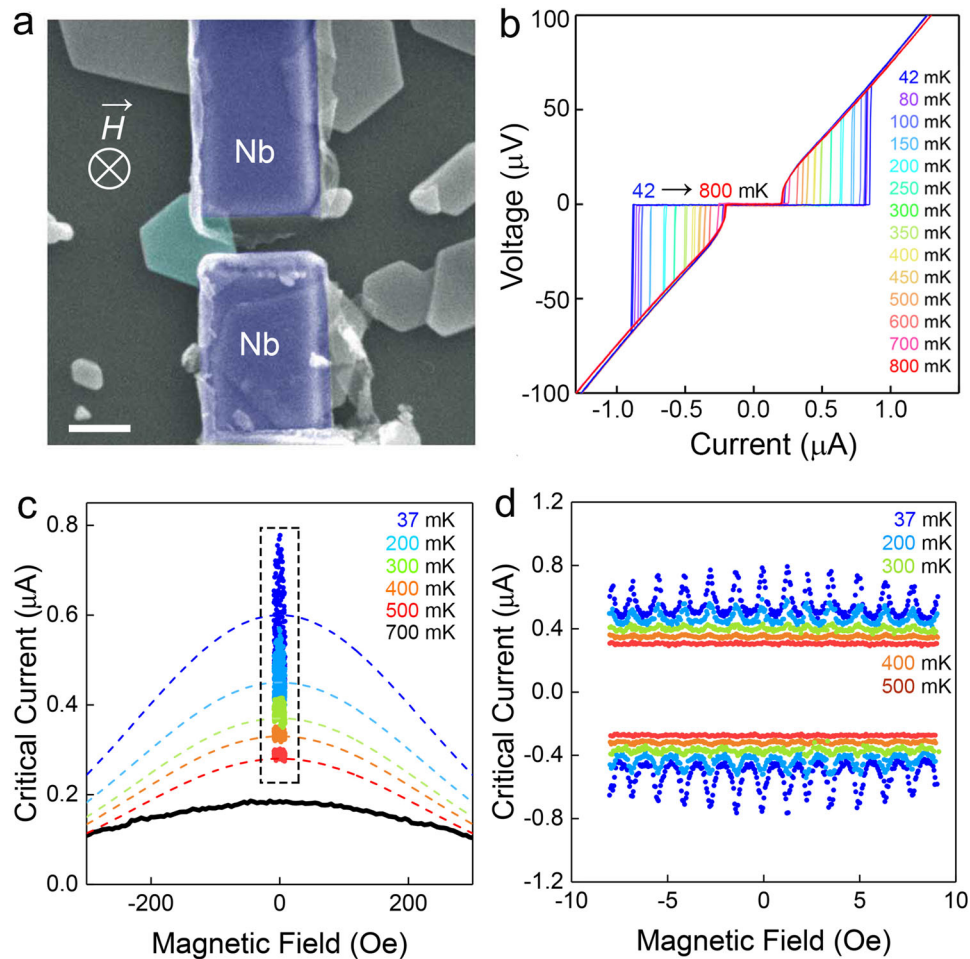


**Figure 1.** Josephson transport through Nb-Bi<sub>2</sub>Te<sub>2.3</sub>Se<sub>0.7</sub>-Nb SNS structure. a) Scanning electron micrograph of the device (the scale bar corresponds to 250 nm). The 28 nm thick nano-crystal and the two Nb-electrodes are colored. b) Below  $\approx 1.2$  K, the current–voltage characteristics are nonlinear and demonstrate jumps typical for Josephson junctions (the retrapping currents are not shown). c) Magnetic field dependence of the critical current  $I_c(H)$  at different temperatures. Black line: a bell-like  $I_c(H)$  (measured at 700 mK) is typical for small lateral Josephson junctions;<sup>[23–25]</sup> color data points:  $I_c(H)$  acquired at low fields  $|H| < 10$  Oe between 500 and 37 mK. Dashed color lines: expected  $I_c(H)$  at higher fields. d) The expanded view of  $I_c(H)$  in (c) reveals tiny oscillations of the critical current with the period  $\approx 1.2$  Oe. The oscillation amplitude sharply rises below 500 mK.

measurements”) were taken on the devices comprising two superconducting niobium (Nb) electrodes attached to a single nano-crystal of Bi<sub>2</sub>Te<sub>2.3</sub>Se<sub>0.7</sub> to form a S–TI–S structure,<sup>[23]</sup> **Figure 1a**. The results of measurements are shown in **Figure 1b–d**. The panel (b) displays the voltage versus current  $V(I)$  characteristics acquired at different temperatures. On these curves, sharp vertical jumps define the critical values of Josephson currents  $I_c$ . Panel (c) represents the overall magnetic field dependence of the critical current; the observed bell-like shape of  $I_c(H)$  is expected for this kind of the SNS junctions.<sup>[24,25]</sup> The central discovery is the fine oscillations  $I_c(H)$ , presented in panel (d), which appear below 500 mK at the top of the generic dependence shown in panel (c). The oscillations have surprisingly short period  $\approx 1.2$  Oe, strong temperature dependence, and very unusual peaked shape, in a striking contrast with the smooth maxima of the commonly observed Fraunhofer-like patterns. Several devices were tested and showed similar oscillations.

The observed oscillations are at odds with the known behaviour of the Josephson junctions. To understand their physical

origin, we start with the detailed examining of the device structure. **Figure 2a** sketches the cross-section of the device. Ultra-thin (10–30 nm) Bi<sub>2</sub>Te<sub>2.3</sub>Se<sub>0.7</sub> nano-crystals were grown by the physical vapor deposition from the original Bi<sub>2</sub>Te<sub>2.3</sub>Se melt. A high transparency of the Nb–TI interfaces was achieved by the in situ RF-plasma Ar-etching of the TI surface prior sputtering Nb-electrodes. Along with the low thickness and high quality of the TI-single crystals, it enables the ballistic transport of the Cooper pairs dominated by the flow along the surface channels of Bi<sub>2</sub>Te<sub>2.3</sub>Se<sub>0.7</sub>.<sup>[23]</sup>

As a result of the Ar-etching, the nano-crystals under the Nb-electrodes get damaged and are characterized by the short electron mean free path.<sup>[26]</sup> Only a few ballistic channels remain well-connected via these damaged regions. Moreover, a band bending is likely to occur in the part of the crystal covered with the Nb electrodes.<sup>[27,28]</sup> As a result, superconducting correlations induced by the proximity under Nb evolve into a strongly diffusive regime (see **Figure 2a**). There, only a small fraction of the Cooper pairs may transform into the triplet  $p$ -wave superconductivity in

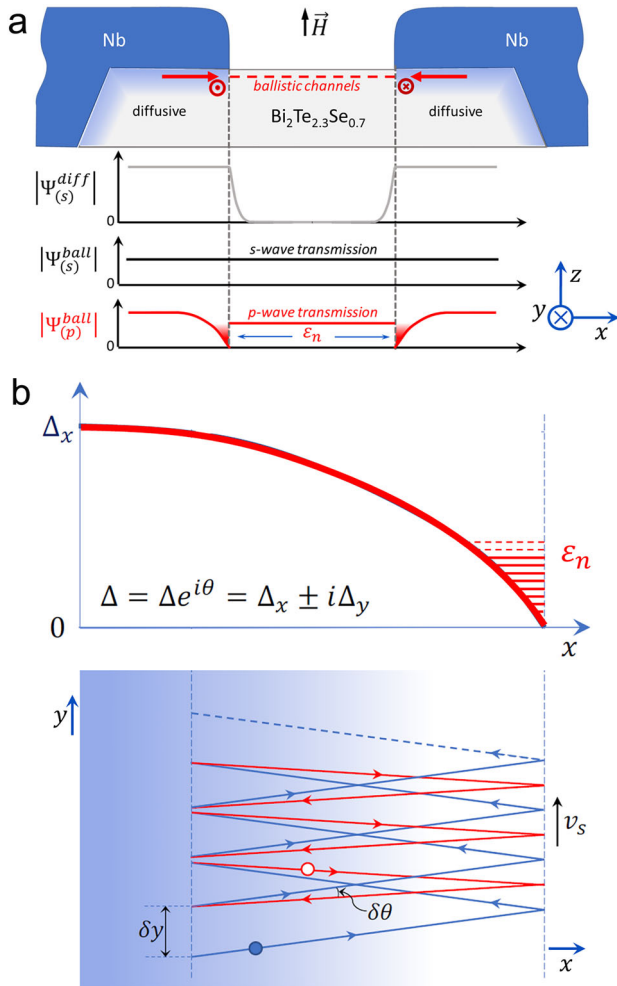


**Figure 2.** Formation of the localized Andreev levels. a) A sketch of the device and the expected spatial evolution of diffusive  $s$ -wave (grey line), ballistic  $s$ -wave (black line), and  $p$ -wave (red line) correlations inside the nano-crystal. b) Upper panel: thick solid line depicts the spatial evolution of the  $x$ -component of the order parameter near diffusive–ballistic interface; thin red lines: set  $\varepsilon_n$  of Andreev levels. Lower panel: Andreev reflection process presented in terms of the geometrical optics approach. The angle of the elemental Doppler shift is  $\delta\theta \approx v_s/v_F$ , see details in the text. The elemental shift  $\delta y$  corresponding to a single cycle of reflection is equal to the electronic wave length, see details in the text. During the multiple reflections, a successive Sommerfeld quantization of the angle  $\delta\theta$  occurs, so that  $\delta y = n\lambda$ , generates a set  $\varepsilon_n$  of the discrete Caroli-de Gennes–Matricon levels.<sup>[32]</sup>

the 2D surface layer within the mean free path distance from Nb electrodes.<sup>[23]</sup> Thus, strongly diffusive  $s$ -wave correlations are dominant in the TI under the electrodes.

In the vicinity of the Nb edges, however, the damaged regions are linked to the pristine central region of  $\text{Bi}_2\text{Te}_{2.3}\text{Se}_{0.7}$ . In this noncovered part of the crystal, the Fermi level is located in the bulk band gap,<sup>[29]</sup> preventing the trivial 3D states to contribute to the electron transport<sup>[23]</sup> (gray curve in Figure 2a). Only a few ballistic surface channels connect the two superconducting electrodes, promoting the transmission of the  $s$ -wave (black curve) and  $p$ -wave (red curve) correlations that both contribute to the supercurrent. Thus, the non-damaged part

of the TI-crystal adjacent to the diffusive ones is a perfect host for the  $p$ -wave modes, allowing for exploring their intriguing consequences.

At the interfaces between the Nb-covered diffusive region and Nb-free ballistic 2D region (vertical dashed lines in Figure 2a) the quasiparticles experience backscattering, due to the Fermi velocity mismatch. For the  $s$ -wave channels, this backscattering is compensated by the diffusive transport near the Nb edge. This well-known “reflectionless tunneling effect”<sup>[30]</sup> provides the high effective transparency for the  $s$ -wave correlations (transparency 1 was used to fit the corresponding conventional contribution to the supercurrent, see Supporting Information section Temperature Evolution of critical current). At the same time, the  $x$ -component of the induced  $p$ -wave order parameter  $\Delta = \Delta_x + i\Delta_y$  is partially suppressed near the interfaces on the scale of the superconducting coherence length  $\xi$  (two dips in red curve in Figure 2a). Figure 2b depicts this evolution for the left interface. There the quantum well formed by vanishing  $\Delta_x$ , on the left side, and by the jump at the interface, on the right side, hosts sub-gap Andreev bound states. In the framework of the semiclassical approximation, such states have a linear energy dispersion versus the wave number  $k_y$  parallel to the interface<sup>[31]</sup>  $\varepsilon = \Delta \sin(k_y y)$ , with the mid-gap state corresponding to  $k_y = 0$ . Note that in general, the  $p$ -wave state is characterized by the presence of either a single or two simultaneously present edge modes. In the former case, one deals with the chiral  $p$ -wave, in the latter case, one has two helical modes with the plus and minus helicities, respectively. Importantly, both modes disperse linearly with momentum and, therefore, the Andreev bound states are equivalent in both cases. Finally, interfaces harbor supercurrents resulting in reconstruction of the Andreev states which we discuss now.

In the following we go beyond the semi-classical approximation. Considering the low transparency of the interface between the superconducting and normal TI, we describe our device as a free-standing  $p$ -wave superconducting specimen; the edges of the specimen represent the above mentioned interfaces in the real device. In the spirit of the Stone’s picture of Andreev reflection,<sup>[32]</sup> the edge supercurrents make the Andreev scattering not perfectly retroreflecting (see lower panel in Figure 2b): Each reflection causes a small change in the angle of the incidence, with  $\delta\theta \approx v_s/v_F \approx \Delta/\varepsilon_F$  in the regime of small angles  $\theta$  or, equivalently, of low quasiparticle energies. Here  $v_s, v_F$  are superfluid and Fermi velocities, respectively, and  $\varepsilon_F$  is the Fermi energy in the proximized 2D TI layer. Within this geometrical optics picture of the Andreev reflection,<sup>[32]</sup> we predict that the linear spectrum near  $\varepsilon = 0$  splits into a set of the discrete low-energy states

$$\varepsilon_n \approx \Delta(v_s/v_F)n \approx (\Delta^2/\varepsilon_F)n \quad (1)$$

where  $n = 1, 2, 3$  is the quantum number which appears as the ratio  $\delta y/\lambda$ , where  $\lambda$  is the electron wavelength. Indeed, since the width of the effective potential well is  $\xi \approx \hbar v_F/\Delta$ , and using  $\varepsilon_F \approx v_F p_F$ , we have  $\delta y \approx \xi \delta\theta \approx (\hbar v_F/\Delta)(\Delta/v_F p_F) \approx \lambda$ , that is, the Bohr–Sommerfeld quantization condition holds. Taking  $\Delta \approx 0.3$  meV and  $\varepsilon_F \approx 0.1$  eV,<sup>[23]</sup> we get an estimate for the inter-level spacing  $\delta\varepsilon_n \approx 1$   $\mu$ eV. Note that similar fine level structure  $\varepsilon_n \approx \Delta^2/\varepsilon_F$  was predicted in the core of an Abrikosov vortex by Caroli, De Gennes, and Matricon,<sup>[33]</sup> beyond the semi-classical Andreev ap-

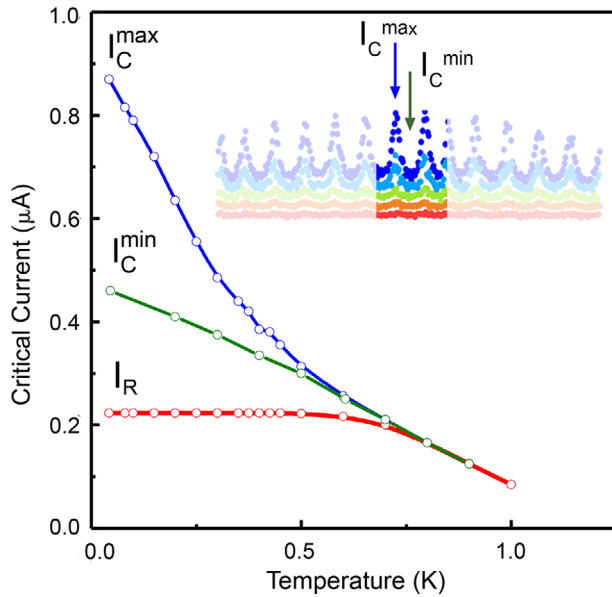


**Figure 3.** Evolution of critical currents with temperature. Blue curve: evolution of the maximum critical current (measured at the first peak at  $H = 0$  Oe). Green curve: evolution of the minimum current (first minimum, at  $H \approx 0.5$  Oe). Red line: retrapping current.

proximation. In case of vortices however,  $v_s$  represents circular supercurrents, whereas in our case it arises due to the Josephson supercurrent component along the electrode edge or else, may be caused by the chiral  $p$ -wave symmetry of the proximity-induced order parameter at the TI surface.

Exactly the same level structure forms at the opposite (right) electrode of our S–TI–S device. We anticipate that it is the transmission between these energy levels by ballistic TI channels that provides the observed anomalous resonant contribution to the Josephson supercurrent, Figure 1d. Earlier, the resonant tunneling via mid-gap Andreev bound states was discussed in the context of junctions between  $d$ -wave<sup>[34]</sup> or  $p$ -wave superconductors.<sup>[35]</sup> Due to the expected fine level structure in

$\mu\text{eV}$  range, very low temperatures below  $\approx 10$  mK are needed to resolve their individual contributions.

Though, an external magnetic field  $H$  applied perpendicularly to the device plane provides a Doppler shift of the levels in the opposite directions in the two electrodes.<sup>[36]</sup> The shift magnitude is  $\delta\epsilon \approx \Delta(H/H_c)$ , where  $H_c = \Phi_0/\pi\xi\lambda_L$  is thermodynamic critical field,  $\xi \approx 100$  nm is the coherence length in the proximized ballistic region and  $\lambda_L \approx 100$  nm is the London penetration depth of Nb (since Nb electrodes provide magnetic field screening). Using these numbers, we get  $H_c \approx 10^3$  Oe, and thus, an external field in the  $\approx 0.1$  Oe range provides a shift  $2\delta\epsilon \approx 10^{-3}\Delta$ , which is indeed of the order of inter-level spacing  $\delta\epsilon_n$ . As a result, periodic out-of-resonance shifts of the levels in low fields (much smaller than  $\approx 500$  Oe needed to provide flux quantum per junction area in Figure 1c) lead to ultra-fine periodic oscillations of the critical current.

The fine period  $\approx \Delta^2/\epsilon_F$  of the observed oscillations is thus consistent with the  $p$ -wave symmetry of the induced order parameter. It also fully excludes the  $s$ -wave symmetry since in the  $s$ -wave case the low energy Andreev bound states do not exist; only the levels  $\approx \Delta$  can form. It should be mentioned for completeness, that another possibility could, in principle, be a  $d$ -wave symmetry when the mid-gap bound states may form if the lobes of the order parameter are misaligned with respect to the interface. However, the level splitting mechanism proposed in our work and illustrated in Figure 2 is not operative in the  $d$ -wave case as the latter has the so-called flat dispersion with the bound levels pinned strictly to zero energy.

The temperature dependence of the oscillation amplitude presented in Figure 3 further supports our prediction. There, the values  $I_c^{\text{min}}$  of the critical current at the minima of oscillations (green open circles) nicely follow the Kulik–Omelyanchuk ballistic behavior<sup>[37,38]</sup> (green curve, see Supporting Information section, Temperature Evolution of critical current), in agreement with the expected  $s$ -wave origin of  $I_c^{\text{min}}$ . The observed upturn in  $I_c^{\text{max}}(T)$  (oscillation maxima) along with a rapid rise of the oscillation amplitude  $I_c^{\text{max}}(T) - I_c^{\text{min}}(T)$  when lowering temperature also supports our model. Indeed, based on considerations developed in refs. [34, 39] one expects the amplitude of this resonant contribution due to  $p$ -component to be  $\propto \Delta^2/T$ . Furthermore, the

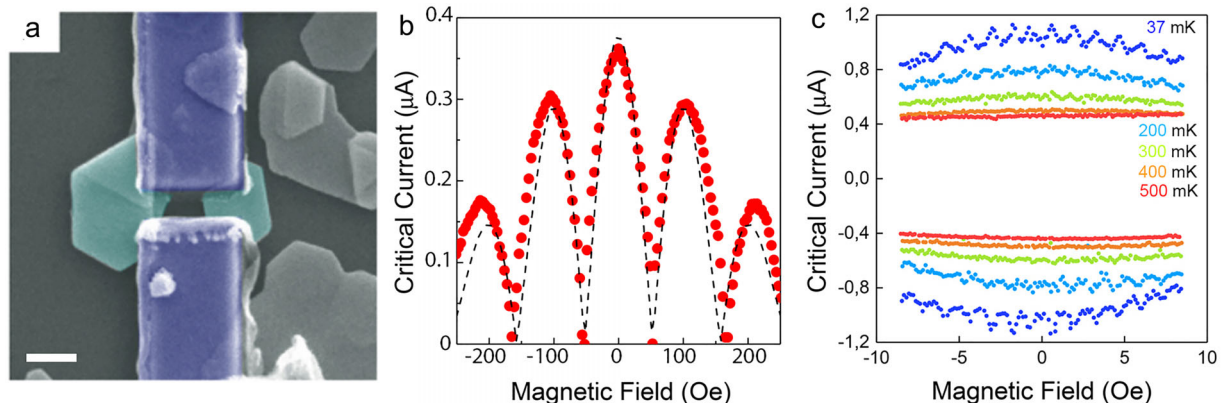


**Figure 4.** Josephson transport through a SQUID-like device. a) Scanning electron micrograph of the device (the scale bar corresponds to 250 nm). Two closely spaced nano-crystals of  $\text{Bi}_2\text{Te}_{2.3}\text{Se}_{0.7}$  (false colored in green) form the SQUID arms. b) Data points: Critical current versus field dependence (here at 700 mK) exhibits oscillations with large periodicity  $\delta H \approx 105$  Oe. Black dashed line: a fit by the Fraunhofer expression for a SQUID (see in the text). c) Below 300 mK and at very low fields,  $I_c(H)$  fine oscillations with periodicity  $\approx 1.3$  Oe are observed.

observed sharp peaks at the maxima of oscillations find their straightforward explanation since the transmission probability is drastically enhanced at the resonance where the levels match. Finally, it is worth to mention the recent study<sup>[40]</sup> which is apparently unrelated to our work, but where qualitatively similar enhancement of critical current at low T was reported in BiSbTeSe<sub>2</sub> nanoribbons and attributed to the contribution of low energy Andreev bound states, though via different mechanism.

Since our explanation is based on a resonance transmission via Andreev levels forming at interfaces, one expects the oscillation period to be rather insensitive to the details of the device geometry. In **Figure 4a**, a device involving two TI-crystals is presented. Expectedly, this device shows overall oscillatory  $I_c(H)$  characteristics typical of a DC-SQUID<sup>[23]</sup> (see **Figure 4b**), very different from the bell-like  $I_c(H)$  of a single junction presented in **Figure 1c**. The oscillations have a large period  $\delta H \approx 105$  Oe and follow Fraunhofer behavior,  $I_c(H) = I_c(0) \left| \frac{\sin(\Phi(H)/\Phi_0)}{\Phi(H)/\Phi_0} \right|$ , where  $\Phi(H) = HS$  is the flux through the SQUID loop of a section  $S$ . A satisfactory fit (black dashed line in **Figure 4b**) is obtained with  $S = 0.2 \mu\text{m}^2 \approx (0.45 \mu\text{m})^2$ , that corresponds well to the physical size of the device in **Figure 4a**. Though, the SQUID-like junction also shows fine oscillations of  $I_c$  at low fields, **Figure 4c**. While the amplitude of these oscillations is lower than in a single-junction device (eventually due to the interference between the contributions of the two arms and/or slightly different interfaces), their periods are quite the same. Note that the oscillation period of  $\approx 1$  Oe would correspond to one flux quantum per area  $S = \Phi_0/1 \text{ Oe} \approx (5 \mu\text{m})^2$  which is more than ten times larger than any dimension of the studied devices. This again excludes any link between the observed oscillations and the conventional flux quantization phenomena.

### 3. Conclusion

The peculiar temperature dependence of the observed oscillations, their characteristic peaked shape and ultra-fine period are, therefore, the direct experimental evidences that support our model of the resonant transmission by ballistic  $p$ -wave topological channels via specific low-lying Andreev levels formed at the two S-TI interfaces of the Josephson junction. Unveiling whether the observed states have chiral or helical nature calls for the next step study. Knowing the precise symmetry of the linear dispersion of Andreev states near the Dirac point will provide a platform for implementing the concrete topological  $p$ -wave based construction of qubits.

### 4. Experimental Section

**Sample Growth:** The growth conditions of Bi<sub>2</sub>Te<sub>2.3</sub>Se<sub>0.7</sub> nano-crystals, S-TI-S device layout, the stages of the device elaborations, their basic structural and electronic properties are presented in details in ref. [23].

**Transport Measurements:** For each studied sample, the transport experiments were carried out in three steps. First, the resistive transition to the superconducting state was recorded, and the evolution of  $I(V)$  characteristics with temperature was studied in zero-magnetic field. Second, the overall  $I_c(H)$  characteristics were measured in fields up to 1 kOe. Third, the experiments revealing fine oscillations were provided. The samples were cooled below the superconducting critical temperature at zero-field. The eventual residual magnetic field of a few Oe remained much lower than the field  $H_{\text{vortex}} > 100$  Oe required to stabilize one vortex in 500 nm wide

Nb electrodes (an even higher field  $H_{\text{vortex}} > 200\text{--}500$  Oe for 200–400 nm large TI-nanocrystals). In this way any possibility for the vortex presence in the junction was excluded. After achieving the required temperature,  $I_c(H)$  characteristics were acquired in a narrow field range  $|H| < 10$  Oe which was also at least ten times lower than the field required for the first vortex penetration inside the device. Thus, the vortex penetration in the device during these experiments was excluded. Independently, the typical symmetric bell-like  $I_c(H)$  dependence in **Figure 1c** confirms that no extra flux influenced the experiments at least up to 300 Oe. This is an additional proof that no flux in Nb or TI was trapped during the cooling or the measurement process.

Taking into account the field profile due to Meissner diamagnetism, the studied junctions used 70 nm thick and 500 nm wide Nb electrodes. The former was close to and the latter larger than the London penetration depth of Nb,  $\approx 100$  nm. At low magnetic fields, the Meissner currents in Nb partially screen the external field  $H$ , so inside Nb  $H_{\text{Nb}} < H$ . Though, the expelled field was refocused at the TI crystal between the two Nb-electrodes. There, the field amplitude was larger than  $H$ . The estimations show that, depending on considered location, the field can be higher or lower than  $H$  by a geometric factor 0.6–1.9.<sup>[23]</sup> At Nb-edges where Andreev bound states were formed and Meissner currents flow, the local field was almost equal to  $H$ . It is also important that this geometric factor was constant in field, that is the relation between local and external field remains linear. Thus, the measured value of the oscillation period may differ from the “theoretical” one by a numeric factor  $\approx 2$ .

**Experimental Setup:** The experiments were carried out on BlueFors LD250 refrigerator. The ultra-low distortion function generator DS360 was used as current source and 24-bit eight-channel ADC-card Leonardo II as a digitizer of voltage, current and magnetic field signals. The voltage signal was preamplified by a home-made symmetric amplifier (voltage noise density 3 nV/ $\sqrt{\text{Hz}}$ ) with the symmetric current biasing of samples. All DC-lines were designed to feature a strong common mode rejection at low frequency (50 Hz and harmonics). The electric connections were filtered using two-stage low-pass RC-filters ( $R = 1 \text{ k}\Omega$ ,  $C = 100 \text{ nF}$ , cut-off frequency of 1.7 kHz), the filter being fixed at 100 mK-plate. The RC-filters were followed by a compact silver-epoxy microwave filter made of twelve 1.6 m long twisted pairs (the so-called TP-filter) where only one line pair was used; the design of the filter and of the thermal sink were those used in millikelvin microwave experiments.<sup>[41]</sup> The TP-filter was located directly on the mixing chamber in the vicinity of the sample holder. The resulted filter efficiency exceeded 150 dB of attenuation in the frequency range 0.1–20 GHz. For 2 month period of measurements, the critical current oscillations of both T-SQUID and TSJ showed stable and reproducible behavior. The total current noise of the measurement setup was tested on single Al/AIO<sub>x</sub>/Al Josephson junctions with the normal resistance of 5 k $\Omega$  and a low theoretical Ambegaokar–Baratoff critical current of 50 nA; the measured switching current was 30 nA. The resulted current noise amplitude was significantly lower than 10 nA and this was not able to influence  $\approx 1 \mu\text{A}$  current oscillations observed in all measured topological structures. The calibrated magnetic field (85 Oe A<sup>-1</sup>) was applied perpendicularly to the sample plane.

### Supporting Information

Supporting Information is available from the Wiley Online Library or from the author.

### Acknowledgements

The authors thank M. Yu. Kupriyanov and Y. Tanaka for fruitful discussions and advice, L. Tagirov and O. Emeyanova for realization of the XPS and EDX analyses of crystals, and D. Lvov and S. Egorov for technical support during the sample fabrication and measurements. The transport experiments were carried out with the support of the RSF-ANR grant CrysTop (20-42-09033). The sample preparation was realized with the support of the

RSF (21-72-00140). D.R. acknowledges COST Action CA16218 - Nanoscale Coherent Hybrid Devices for Superconducting Quantum Technologies, French ANR grant SUPERSTRIPES. V.L.G. acknowledges support by the State task 075-00475-19-00 IMT RAS. The work of V.M.V. was supported by Terra Quantum AG. A.A.G. acknowledges support by the European Union H2020-WIDESPREAD-05-2017-Twinning project SPINTECH under Grant Agreement No. 810144. This work was partially supported by the Ministry of Science and Higher Education of the Russian Federation (No. FSMG-2021-0005).

## Conflict of Interest

The authors declare no conflict of interest.

## Author Contribution

V.S.S. suggested the idea of the experiment; V.S.S. conceived the project and supervised the experiments; V.S.S. and D.S.Y. grew the nanocrystals, V.S.S. and O.V.S. realized e-beam lithography and thin film deposition, V.L.G., V.S.S. provided the experiment, V.M.V., A.A.G., S.N.K, D.R., and V.S.S. constructed the model of the observed effects; V.S.S., D.R, V.M.V., and A.A.G. wrote the manuscript with the contributions from other authors.

## Data Availability Statement

The data that support the findings of this study are available in the Supporting Information of this article.

## Keywords

andreev bound state, Josephson junction, topological insulator

Received: September 24, 2021

Revised: December 22, 2021

Published online:

- [1] R. Balian, N. R. Werthamer, *Phys. Rev.* **1963**, *131*, 1553.
- [2] M. Sigrist, K. Ueda, *Rev. Mod. Phys.* **1991**, *63*, 239.
- [3] A. P. Mackenzie, Y. Maeno, *Rev. Mod. Phys.* **2003**, *75*, 657.
- [4] C. W. J. Beenakker, *Annu. Rev. Condens. Matter Phys.* **2013**, *4*, 113.
- [5] M. Sato, Y. Ando, *Rep. Prog. Phys.* **2017**, *80*, 076501.
- [6] J. Alicea, *Rep. Prog. Phys.* **201**, *75*, 076501.
- [7] S. M. Frolov, M. J. Manfra, J. D. Sau, *Nat. Phys.* **2020**, *16*, 718.
- [8] L. Fu, C. L. Kane, *Phys. Rev. Lett.* **2008**, *100*, 096407.
- [9] M. Sato, S. Fujimoto, *Phys. Rev. B* **2009**, *79*, 094504.
- [10] Y. Tanaka, T. Yokoyama, N. Nagaosa, *Phys. Rev. Lett.* **2009**, *103*, 107002.
- [11] X.-L. Qi, S.-C. Zhang, *Rev. Mod. Phys.* **2011**, *83*, 1057.
- [12] G. Tkachov, E. N. Hankiewicz, *Phys. Rev. B* **2013**, *88*, 075401.
- [13] B. Sacépé, J. B. Oostinga, J. Li, A. Ubal dini, N. J. G. Couto, E. Giannini, A. F. Morpurgo, *Nat. Commun.* **2011**, *2*, 575.
- [14] M. Veldhorst, M. Snelder, M. Hoek, T. Gang, V. K. Guduru, X. L. Wang, U. Zeitler, W. G. van der Wiel, A. A. Golubov, H. Hilgenkamp, A. Brinkman, *Nat. Mater.* **2012**, *11*, 417.
- [15] J. B. Oostinga, L. Maier, P. Schüffelgen, D. Knott, Ch. Ames, Ch. Brüne, G. Tkachov, H. Buhmann, L. W. Molenkamp, *Phys. Rev. X* **2013**, *3*, 021007.
- [16] J. R. Williams, A. J. Bestwick, P. Gallagher, Seung Sae Hong, Y. Cui, Andrew S. Bleich, J. G. Analytis, I. R. Fisher, D. Goldhaber-Gordon, *Phys. Rev. Lett.* **2012**, *109*, 056803.
- [17] L. Galletti, S. Charpentier, M. Iavarone, P. Lucignano, D. Massarotti, R. Arpaia, Y. Suzuki, K. Kadowaki, T. Bauch, A. Tagliacozzo, F. Tafuri, F. Lombardi, *Phys. Rev. B* **2014**, *89*, 134512.
- [18] E. Bocquillon, R. S. Deacon, J. Wiedenmann, P. Leubner, T. M. Klapwijk, C. Brüne, K. Ishibashi, H. Buhmann, L. W. Molenkamp, *Nat. Nanotechnol.* **2017**, *12*, 137.
- [19] S. Charpentier, L. Galletti, G. Kunakova, R. Arpaia, Y. Song, R. Baghdadadi, S. Min Wang, A. Kalaboukhov, E. Olsson, F. Tafuri, D. Golubev, J. Linder, T. Bauch, F. Lombardi, *Nat. Commun.* **2017**, *8*, 2019.
- [20] S. Ghatak, O. Breunig, F. Yang, Z. Wang, A. A. Taskin, Y. Ando, *Nano Lett.* **2018**, *18*, 5124.
- [21] J. Wiedenmann, E. Bocquillon, R. S. Deacon, S. Hartinger, O. Herrmann, T. M. Klapwijk, L. Maier, C. Ames, C. Brüne, C. Gould, A. Oiwa, K. Ishibashi, S. Tarucha, H. Buhmann, L. W. Molenkamp, *Nat. Commun.* **2016**, *7*, 10303.
- [22] C. Li, J. C. de Boer, B. de Ronde, Shyama V. Ramankutty, E. van Heumen, Y. Huang, A. de Visser, A. A. Golubov, M. S. Golden, A. Brinkman, *Nat. Mater.* **2018**, *17*, 875.
- [23] V. S. Stolyarov, D. S. Yakovlev, S. N. Kozlov, O. V. Skryabina, D. S. Lvov, A. I. Gumarov, O. V. Emelyanova, P. S. Dzhumaev, I. V. Shchetinin, R. A. Hovhannisyan, S. V. Egorov, A. M. Kokotin, W. V. Pogosov, V. V. Ryazanov, M. Yu. Kupriyanov, A. A. Golubov, D. Roditchev, *Commun. Mater.* **2020**, *1*, 38.
- [24] O. V. Skryabina, S. V. Egorov, A. S. Goncharova, A. A. Klimenko, S. N. Kozlov, V. V. Ryazanov, S. V. Bakurskiy, M. Yu. Kupriyanov, A. A. Golubov, K. S. Napolskii, V. S. Stolyarov, *Appl. Phys. Lett.* **2017**, *110*, 222605.
- [25] J. C. Cuevas, F. S. Bergeret, *Phys. Rev. Lett.* **2007**, 217002.
- [26] V. S. Stolyarov, V. A. Sheina, D. A. Khokhlov, S. Vlaic, S. Pons, H. Aubin, R. S. Akzyanov, A. S. Vasenko, T. V. Menshchikova, E. V. Chulkov, A. A. Golubov, T. Cren, D. Roditchev, *J. Phys. Chem. Lett.* **2021**, *12*, 3127.
- [27] V. S. Stolyarov, S. V. Remizov, D. S. Shapiro, S. Pons, S. Vlaic, H. Aubin, D. S. Baranov, Ch. Brun, L. V. Yashina, S. I. Bozhko, T. Cren, W. V. Pogosov, D. Roditchev, *Appl. Phys. Lett.* **2017**, *111*, 251601.
- [28] V. S. Stolyarov, S. Pons, S. Vlaic, S. V. Remizov, D. S. Shapiro, C. Brun, S. I. Bozhko, T. Cren, T. V. Menshchikova, E. V. Chulkov, W. V. Pogosov, Y. E. Lozovik, D. Roditchev, *J. Phys. Chem. Lett.* **2021**, *12*, 9068.
- [29] D. O. Scanlon, P. D. C. King, R. P. Singh, A. de la Torre, S. McKeown Walker, G. Balakrishnan, F. Baumberger, C. R. A. Catlow, *Adv. Mater.* **2012**, *24*, 2154.
- [30] B. J. van Wees, P. de Vries, P. Magnee, T. M. Klapwijk, *Phys. Rev. Lett.* **1992**, *69*, 510.
- [31] A. Furusaki, M. Matsumoto, M. Sigrist, *Phys. Rev. B* **2001**, *64*, 054514.
- [32] M. Stone, *Phys. Rev. B* **1996**, *54*, 13222.
- [33] C. Caroli, P. G. de Gennes, J. Matricon, *J. Phys. Lett.* **1964**, *9*, 307.
- [34] Y. Tanaka, S. Kashiwaya, *Phys. Rev. B* **1997**, *56*, 892.
- [35] H.-J. Kwon, V. M. Yakovenko, K. Sengupta, *Low Temp. Phys.* **2004**, *30*, 613.
- [36] L. A. B. Olde Olthof, S.-I. Suzuki, A. A. Golubov, M. Kunieda, S. Yonezawa, Y. Maeno, Y. Tanaka, *Phys. Rev. B* **2018**, *98*, 014508.
- [37] I. O. Kulik, A. N. Omel'anchuk, *Sov. J. Low Temp. Phys.* **1977**, *3*, 459.
- [38] A. A. Golubov, M. Yu. Kupriyanov, E. Il'ichev, *Rev. Mod. Phys.* **2004**, *76*, 411.
- [39] E. Il'ichev, M. Grajcar, R. Hlubina, R. P. J. IJsselsteijn, H. E. Hoenig, H.-G. Meyer, A. Golubov, M. H. S. Amin, A. M. Zagorskin, A. N. Omelyanchouk, M. Yu. Kupriyanov, *Phys. Rev. Lett.* **2001**, *86*, 5369.
- [40] M. Kayyalha, M. Kargarian, A. Kazakov, I. Miotkowski, V. M. Galitski, V. M. Yakovenko, L. P. Rokhinson, Y. P. Chen, *Phys. Rev. Lett.* **2019**, *122*, 047003.
- [41] C. P. Scheller, S. Heizmann, K. Bedner, D. Giss, M. Meschke, D. M. Zumbuhl, J. D. Zimmerman, A. C. Gossard, *Appl. Phys. Lett.* **2014**, *104*, 211106.